ACS Catalysis

RESEARCH ARTICLE

pubs.acs.org/acscatalysis

Catalysis Science of Methanol Oxidation over Iron Vanadate Catalysts: Nature of the Catalytic Active Sites

Kamalakanta Routray,[†] Wu Zhou,[‡] Christopher J. Kiely,[‡] and Israel E. Wachs*[,†]

[†]Operando Molecular Spectroscopy and Catalysis Laboratory, Department of Chemical Engineering and [‡]Department of Materials Science and Engineering, Lehigh University, Bethlehem, Pennsylvania, 18015

Supporting Information

ABSTRACT: Bulk mixed metal oxides are widely used in industry for various oxidation reactions, but there is still debate in the heterogeneous catalysis literature about the nature of their catalytic active sites. In the present study, the two-component iron vanadate mixed metal oxide system is employed to investigate the outermost surface composition and surface chemistry of the bulk $FeVO_4$ mixed metal oxide catalyst. The bulk V_2O_5, α-Fe_2O_3, and supported 4% V_2O_5/α-Fe_2O_3 metal oxide systems were also investigated to better understand the surface composition and surface chemistry of the bulk $FeVO_4$ catalyst. Raman spectroscopy confirmed that the bulk $FeVO_4$ was phase pure and has no contribution from excess V_2O_5 and α-Fe_2O_3 phases. IR spectroscopy confirmed that the model supported 4% V_2O_5/α-Fe_2O_3 catalyst consists of an amorphous surface VO_x monolayer on the α-Fe_2O_3 support. The surface chemistry of the metal oxides was chemically probed with temperature programmed CH_3OH-IR spectroscopy and revealed that both intact surface CH_3OH^* and CH_3O^* species are present on the catalysts. On acidic α-Fe_2O_3, the surface CH_3OH^* and CH_3O^* intermediates yield CH_3OH and dimethyl ether (DME), respectively. For the redox V_2O_5, $FeVO_4$ and supported 4% V_2O_5/α-Fe_2O_3 catalysts: however, both surface intermediates primarily give rise to HCHO. These results confirm that the surface of bulk $FeVO_4$ and supported 4% V_2O_5/α-Fe_2O_3 catalysts are similar and that surface VO_x species are the catalytic active sites for methanol oxidation to formaldehyde over bulk $FeVO_4$ catalysts. This conclusion is supported by HR-TEM images that reveal an amorphous VO_x enriched layer of ∼1 nm at the outer surface of the bulk $FeVO_4$ catalysts. Methanol oxidation over bulk $FeVO_4$ was found to proceed via a Mars−van Krevelen mechanism, where the reduced surface VO_x species are reoxidized by bulk lattice oxygen rather than gas phase molecular O_2. This study demonstrates that the catalytic active sites for oxidation reactions over the bulk $FeVO_4$ mixed oxide reside in the outermost surface layer and not in the bulk lattice structure.

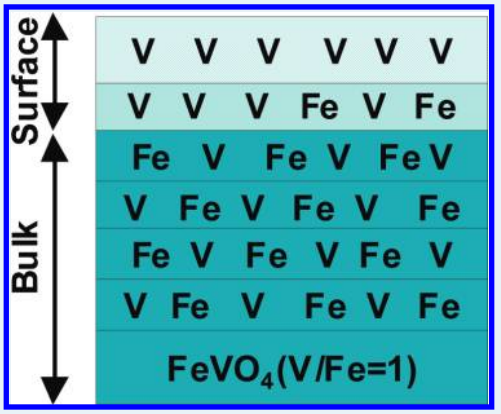

KEYWORDS: oxidation, methanol (CH_3OH), formaldehyde (HCHO), dimethyl ether (CH_3OCH_3), carbon monoxide (CO), carbon dioxide (CO_2), catalysts, bulk, V_2O_5, α-Fe_2O_3, $FeVO_4$, supported, V_2O_5/α-Fe_2O_3, spectroscopy, in situ, Raman, IR, TPSR, microscopy, electron, HR-TEM, EELS

1. INTRODUCTION

Bulk mixed metal oxides with two or more metals are widely used as commercial catalysts for various processes in the petrochemical industry.[1−5] A few examples of two-component bulk mixed metal oxide catalysts are bismuth molybdate and iron molybdate. Bulk bismuth molybdate selectively oxidizes propylene to acrolein and acrylic acid[1] and iron molybdate selectively oxidizes methanol to formaldehyde.[2] Bulk V−P−O catalysts are employed for the oxidation of *n*-butane to maleic anhydride.[6] Examples of three and four component bulk mixed metal oxides are the Mo−V−Nb−O and M−V−Nb−Te−O catalysts that are effective for oxidative dehydrogenation of propane to propylene and ammoxidation of propane to acrylonitrile, respectively.[3,4] Despite the wide industrial application of bulk mixed metal oxide catalysts, the origin of the enhanced catalytic activity and selectivity of bulk mixed metal oxides is still not fully understood and continues to be debated in the catalysis literature.[5] The absence of detailed surface information about the bulk mixed metal oxides has primarily been responsible for the lack of scientific progress in this field. Given that the bulk mixed metal oxides readily lend themselves to bulk characterization, bulk spectroscopic techniques (XRD, TEM, Neutron Diffraction, EXAFS/XANES, solid state NMR, UV−vis, IR and Raman spectroscopy) have almost exclusively been employed in their characterization. In contrast, the limited surface information about the catalytic active sites has hampered the establishment of fundamental structure−activity/selectivity relationships for bulk mixed metal oxide catalysts.

Received: October 23, 2010
Revised: November 23, 2010
Published: December 20, 2010

The ability of low energy ion scattering (LEIS) spectroscopy to provide information about the outermost layer of a catalyst, ~0.2 nm, makes it the technique of choice for surface characterization of bulk mixed metal oxide catalysts.[7] Although LEIS studies of bulk mixed metal oxide catalysts are rather limited at present, several important findings have recently been reported. LEIS spectroscopic characterization of bulk mixed metal vanadates and molybdates have found that their surfaces are enriched with vanadium and molybdenum, respectively.[8] Guliants et al. have similarly found that for the bulk Mo−V−Te−Nb−O catalyst the surface is enriched with vanadium and molybdenum.[9]

Bulk vanadates have received attention for their catalytic activity and selectivity toward oxidation of methanol to formaldehyde because of their higher activity and less likelihood of decomposition at higher temperatures as compared to bulk mixed metal molybdates.[10,11] Among the bulk vanadates, bulk $FeVO_4$ is interesting because of its structural similarity to the industrial bulk iron molybdate catalyst ($Fe_2(MoO_4)_3$).[12] The crystal structure of the bulk $FeVO_4$ sample used in this study was confirmed with XRD and its phase purity, absence of V_2O_5 nanoparticles, with Raman spectroscopy.[10] The number of exposed catalytic active sites were determined with CH_3OH chemisorption and used to calculate the turnover frequency (TOF) for methanol oxidation.[10,13] Methanol oxidation chemical probe studies revealed that only surface redox sites are present on the bulk $FeVO_4$.[10,14] In spite of these studies, the molecular details of methanol oxidation by bulk $FeVO_4$ catalysts still have not been resolved.

To obtain additional fundamental insights about the molecular level details of bulk mixed metal oxide catalysts in selective oxidation reactions, the model bulk iron vanadate two-component bulk mixed metal oxide system was chosen for the CH_3OH oxidation to HCHO reaction. The catalysts employed in this investigation consisted of bulk $FeVO_4$, V_2O_5, α-Fe_2O_3 and a model vanadium oxide supported on α-Fe_2O_3 (VO_x/α-Fe_2O_3). The structures and phase purity of the catalytic materials were confirmed with Raman spectroscopy. The CH_3OH oxidation reaction was chosen because methanol is a "smart" chemical probe molecule that can discriminate between different types of surface sites (redox, acid, or base),[15,16] distinguish between the different coordinated surface cations (Fe vs V), and also determine the number of exposed surface catalytic active sites (Ns).[16,17] Special emphasis has been placed on obtaining surface information by employing *operando* IR-temperature programmed surface reaction (TPSR) spectroscopy with the CH_3OH chemical probe molecule.

2. EXPERIMENTAL SECTION

2.1. Catalyst Synthesis. The bulk $FeVO_4$ was synthesized by coprecipitation through an organic route using the precursors iron nitrate ($Fe(NO_3)_3 \cdot 9H_2O$; Alfa Aesar Products, 99.9%), ammonium vanadium oxide (NH_4VO_3; Alfa Aesar Products, 99.9%), and citric acid ($HOC(COOH)(CH_2COOH)_2 \cdot H_2O$; Alpha Aesar Products, 99.9%). To 200 mL of distilled water, 5 g of ferric nitrate and 2.5 g of citric acid were added and mixed until the complete dissolution of salts. Citric acid was added to ensure that the molar number of equivalent anions equaled that of cations. About 1.45 g of NH_4VO_3 was separately added to 200 mL of distilled water and then mixed with the 200 mL of distilled water−citric acid−nitrate solution. The mixture was dried in a steam bath until a glassy textured solid was observed. The solid were further dried overnight at a temperature of 70 °C, subsequently, ground and calcined at 550 °C for 4 h to obtain a crystalline material.[10] Commercial α-Fe_2O_3 (Alfa Aesar Products, 99.9%) was calcined at 300 °C in air for 2 h prior to being used as support for synthesis of the supported V_2O_5/α-Fe_2O_3 samples. The supported V_2O_5/α-Fe_2O_3 catalyst was prepared by incipient wetness impregnation of 2-propanol solutions of vanadium isopropoxide ($VO-(O-Pr^i)_3$, Alfa-Aesar 97% purity). The preparation was carried out inside a glovebox under the continuous flow of N_2. After the impregnation of the desired amount of vanadium isopropoxide and 2-propanol solution, the sample was kept inside the glovebox with flowing N_2 overnight. The sample was subsequently dried in flowing N_2 at 120 °C for 1 h and subsequently at 300 °C for 1 h. The sample was then calcined in flowing air at 400 °C for 4 h to yield the supported 4% V_2O_5/α-Fe_2O_3 catalyst.[18] The bulk vanadium oxide was synthesized by thermal decomposition of NH_4VO_3 at 300 °C for 4 h.[13,17]

2.2. BET Specific Surface Area. The BET surface area of the catalyst samples was measured by nitrogen adsorption−desorption in flowing N_2 at −196 °C with a Quantasorb surface area analyzer (Quantachrome Corporation, model OS-9). A sample quantity of ~0.3 g was typically employed for the measurement, and the sample was outgassed at 250 °C before N_2 adsorption (Quantachrome Corporation, model QT-3).

2.3. Raman Spectroscopy. The Raman studies were performed with a Horiba-Jobin Yvon LabRam-IR High Resolution spectrometer equipped with a 532 nm visible laser source (Yag double-diode pumped laser, coherent 315 m, 20 mW). The Raman spectrometer was equipped with a confocal microscope (Olympus BX-30), notch filter (532 nm), 50× objective, and single-stage monochromator with 900 grooves/mm grating. The Raman spectral resolution was better than 2 cm^{-1}. The laser power was 20 mW at the sample so as to minimize any laser-induced alterations of the sample. The scattered light from the sample was passed through the monochromator grating and collected with a visible sensitive LN_2-cooled CCD detector (Horiba−Jobin Yvon CCD-3000 V). The LabSpec 5 software was used to operate the experimental set up and collect the Raman spectra. The Raman spectra of bulk V_2O_5 and $FeVO_4$ catalysts were collected under ambient conditions as loose powder. The Raman spectra of the α-Fe_2O_3 support and supported 4% V_2O_5/α-Fe_2O_3 were collected under dehydrated conditions using the in situ environmental reaction cell (Linkam T 1500). The α-Fe_2O_3 and supported V_2O_5/α-Fe_2O_3 catalysts were maintained as loose powder and dehydrated at 400 °C for 30 min under flowing 10% O_2/Ar (Airgas, ultrahigh purity and hydrocarbon-free) environment. After the catalysts were cooled to 100 °C under the oxidized environment, the Raman spectra of the dehydrated samples were collected.

2.4. FT-IR Spectroscopy. The IR spectra were obtained with an FT-IR spectrometer (SensIR) attachment on the Horiba-Jobin Yvon LabRam-IR high-resolution spectrometer system. The LabRam-IR spectrometer allowed for the same catalyst spot analysis for Raman and FT-IR spectroscopy. The FT-IR spectra were collected in the diffuse reflectance mode by use of a total-reflecting objective (Cassegrain/Schwarzschild type). The mid-IR (400−4000 cm^{-1}) spectra were recorded with an MCT detector at a spectral resolution of 4 cm^{-1} using 100 signal-averaged scans. About ~5−10 mg of loose powder was typically placed in the environmental cell, equipped with a CaF_2 window, to perform in situ IR, as well as temperature-programmed reaction studies. The procedures for sample pretreatment and exposure

dx.doi.org/10.1021/cs1000569 |ACS Catal. 2011, 1, 54–66

to different gaseous environments are described in detail in the CH_3OH-TPSR spectroscopy section below. The IR spectra were collected by using QualId-IR software (version 2) manufactured by SensIR Technologies. The FT-IR spectra presented in this paper were background subtracted with spectra collected at 100 °C under a flowing 10% O_2/Ar environment.

The IR spectra of the model supported 4% V_2O_5/α-Fe_2O_3 catalyst were also collected under ambient and dehydrated conditions. The spectra were obtained with a Thermo Nicolet 8700 FT-IR spectrometer equipped with a Harrick Praying Mantis attachment (model DRA-2) for diffuse reflectance spectroscopy. Approximately 30 mg of each sample in powder form was loaded into the cup of the Harrick cell (model HVC-DR2 with a CaF_2 window). The IR spectrum of the hydrated catalyst was collected under ambient conditions. The sample was subsequently heated at a rate of 10 °C/min (Harrick ATC/low voltage temperature control unit) in the Harrick cell to 400 °C and held for 45−60 min under 30 mL/min flowing 10% O_2/Ar (Airgas, certified, 10.00% O_2/Ar balance) before cooling to room temperature. The IR spectra were collected every 90 s using a DTGS detector with a resolution of 4 cm^{-1} and an accumulation of 72 scans. The spectral cutoff for our cell window is about 800 cm^{-1}. The collection of the initial IR gas phase background was performed by placing a reflective mirror in the laser path, while using the Harrick Praying Mantis attachment, at approximately the same height as a full sample cup of the Harrick Cell.

2.5. High-Resolution Transmission Electron Microscopy (HR-TEM). Samples for TEM analysis were prepared by dispersing the catalyst powder in high purity ethanol, and then allowing a drop of the suspension to evaporate onto a lacy carbon film supported by a 300 mesh copper TEM grid. Conventional bright field (BF) TEM images of the samples were collected on a JEOL 2000FX TEM operating at 200 kV. High-resolution TEM (HR-TEM) imaging was performed on a 200 kV JEOL 2200FS (S)TEM equipped with an in-column Ω-filter and having a point-to-point resolution in TEM mode of 0.19 nm.[19] Elemental analysis of the catalyst samples was carried out using electron energy loss spectroscopy (EELS) in scanning mode. Low electron dose settings were used during electron microscopy characterization to minimize electron beam irradiation modification to the samples.

2.6. CH_3OH-TPSR Spectroscopy. The CH_3OH temperature-programmed surface reaction (TPSR) spectroscopy experiments were performed on an Altamira Instruments system (AMI-200) connected to an online Dymaxion Dycor mass spectrometer (DME200MS) for residual gas analysis of reaction products. The execution of the experiment, as well as the collection of data, was done by the "Dycor System 200" software. Typically about ∼250 mg of catalyst was loaded into a U-tube sample holder. The sample was initially dehydrated to remove adsorbed moisture by heating up to 350 °C for 40 min in air (Ultra Zero grade, flow rate = 25 sccm). The sample was then cooled down in flowing air to 110 °C and further cooled in flowing He for an additional 30 min. The flowing helium step assured that the system was purged of air. Subsequently, methanol was adsorbed on the catalyst at 100 °C from a gas stream of 2000 ppm CH_3OH in He (Airgas, Spec grade) for 30 min. The adsorption temperature of 100 °C was selected based on earlier work, which has shown negligible physisorption of CH_3OH at this temperature since physically adsorbed CH_3OH desorbs below 100 °C.[20] The catalyst sample containing the chemisorbed methanol was then flushed with flowing He for another 60 min to remove trace amounts of CH_3OH present in the line and possibly weakly adsorbed methanol. At the same time, the filament of the mass spectrometer was switched on to provide enough time for stabilizing the signal. The CH_3OH-TPSR spectroscopy experiment was then initiated in the flowing He (30 sccm) by increasing the temperature at a rate of 10 °C/min until 400 °C. Blank reactions were performed to confirm the absence of any contribution from the glass U-tubes and from the line between the catalyst bed and the online MS. The gas line connecting the exhaust gases from the TPSR unit to the mass spectrometer (MS) was maintained at ∼130 °C to avoid condensation of products and reactant methanol. It was also determined that for the above experimental conditions complications because of readsorption, concentration gradient in particles, lag times because the diffusion and hold-up in the sample are minimal.[14,21]

Cyclic experiments were performed to check the reaction mechanism of catalysts by performing continuous adsorption and desorption cycles without exposing the sample to the gas phase or ambient O_2. After the completion of first cycle of adsorption and desorption, the MS was turned off and the sample was allowed to cool down in flowing Ar environment from 400 to 100 °C and maintained at 100 °C for 30 min. Methanol was then adsorbed at 100 °C for 30 min, the line was purged with He and the MS was switched on for stabilization. Subsequently, the temperature was ramped up to 400 °C with Ar while the products were analyzed in the mass spectrometer. Typically three adsorption−desorption cycles were performed for samples in the cyclic TPSR experiment.

All the oxidation products, as well as unconverted methanol, were detected on the basis of their m/e numbers in the mass spectrometer. The m/e values employed for detection of various products were as follows: CH_3OH (methanol) = 31, HCHO (formaldehyde) = 30, CH_3OCH_3 (dimethyl ether/DME) = 45, CH_3OOCH (methyl formate/MF) = 60, $(CH_3O)_2CH_2$ (dimethoxy methane/DMM) = 75, H_2O (water) = 18, CO (carbon monoxide) = 28, and CO_2 (carbon dioxide) = 44. The HCHO m/e = 30 mass spectrometer signal was corrected for the small CH_3OH m/e = 30 cracking contribution in the MS. Formation of CO and CO_2 was also observed during the CH_3OH-TPSR experiments and is related to readsorption of HCHO and its subsequent oxidation via surface formates (HCOO*).[20] The HCHO/CH_3OH-TPSR spectra were further analyzed for their surface kinetic information. The first-order Redhead equation was applied to calculate the activation energy, E_a, for HCHO formation[22]

$$\frac{E_a}{RT_P^2} = \frac{\nu}{\beta}\exp\left(-\frac{E_a}{RT_P}\right) \quad (1)$$

in which E_a = activation energy for the reaction (kcal/mol), R = universal gas constant (kcal/kmol K), T_P = desorption peak maximum temperature (K), ν = pre-exponential factor (s^{-1}), and β = heating rate = 10 K min^{-1}.

Previous work on methanol oxidation has shown that the formation of HCHO from CH_3OH follows first-order reaction kinetics in methanol partial pressure.[17] Therefore, the typical first-order $\nu = 10^{13}$ s^{-1} value was used for the calculation of activation energy, E_a, from eq 1.[22] The use of the first-order $\nu = 10^{13}$ s^{-1} value was also confirmed by recent DFT calculations for methanol oxidation over VO_x-based catalysts.[23] This allowed for

dx.doi.org/10.1021/cs1000569 |ACS Catal. 2011, 1, 54–66

calculation of the first-order rate constant for the rate-determining-step (rds), k_{rds}, from the relationship

$$k_{rds}\ (s^{-1}) = 10^{13} \exp\left(-\frac{E_a}{RT_{ref}}\right) \quad (2)$$

in which T_{ref} is the reference temperature used for comparative purposes, which was 230 °C.

2.7. Steady-State Methanol Oxidation. Steady-state methanol oxidation studies over bulk α-Fe_2O_3, bulk V_2O_5, bulk $FeVO_4$, and supported 4% V_2O_5/α-Fe_2O_3 catalysts were performed in an isothermal fixed-bed reactor under atmospheric pressure at a temperature of 230 °C. A reactant stream of CH_3OH/O_2/He with molecular composition of 6/13/81 and a total flow rate of 100 mL/min was flowed through the reactor. An online HP 5890II GC equipped with Carboxene-1000 packed and CP-sil 5 CB capillary columns for TCD and FID detectors, respectively, was employed to analyze the reactants and products. About 10−100 mg of sample was placed in a quartz reactor (ID = 0.35 in.) and treated with O_2/He stream at 300 °C for 30 min prior to the reaction. Methanol was subsequently introduced to the reactor maintained at 230 °C to perform oxidation reaction. Three experimental reaction runs were taken at 230 °C to ensure the reproducibility of the data. During the process care was taken to avoid heat and mass transfer limitations.[24] The methanol conversion, product selectivity and catalyst activity at the corresponding reaction temperature were calculated from the experimental reaction data. Blank runs were also performed to confirm the absence of any catalytic activity of the quartz reactor.

The CH_3OH adsorption equilibrium constant, K_{ads} (atm^{-1}), is determined by combining the k_{rds} values from CH_3OH-TPSR and the corresponding TOF values from the steady-state reaction kinetics

$$\text{TOF}\ (s^{-1}) = k_{rds}K_{ads}P_{CH_3OH} \quad (3)$$

where K_{ads} is the CH_3OH adsorption equilibrium constant and P_{CH_3OH} is the partial pressure of methanol (atm).

3. RESULTS

3.1. BET Surface Area. The BET surface areas of bulk α-Fe_2O_3, V_2O_5, $FeVO_4$, and supported 4% V_2O_5/α-Fe_2O_3 catalysts are presented in Table 1. Bulk V_2O_5 possesses a low surface area of 3.5 m^2/g, and bulk α-Fe_2O_3 has a modest surface area of 23 m^2/g. The surface area of the supported 4% V_2O_5/α-Fe_2O_3 is also 23 m^2/g and reflects the stability of α-Fe_2O_3 support toward calcination upon the impregnation of small amounts of vanadium oxide. The stoichiometric $FeVO_4$ compound has a modest BET surface area of 8 m^2/g, which is twice the surface area of bulk V_2O_5. The BET surface area of bulk V_2O_5, obtained from calcination of NH_4VO_3, at 400 and 450 °C is approximately 4 m^2/g.[13,17]

3.2. Raman and Infrared Spectroscopy. Raman spectroscopy was used to examine the metal oxide phases present in the synthesized catalysts. The Raman spectra of bulk α-Fe_2O_3, V_2O_5, $FeVO_4$, and supported 4% V_2O_5/α-Fe_2O_3 are presented in Figure 1a. The Raman spectrum of the dehydrated α-Fe_2O_3 support possesses sharp bands at 607, 498, 406, 288, 241, and 222 cm^{-1} that are characteristic of the α-Fe_2O_3 phase.[25] The Raman spectrum of bulk V_2O_5 exhibits bands at 994, 700, 523, 477, 402, 299, and 279 cm^{-1} reflecting the crystalline V_2O_5 phase.[26] The Raman spectrum of the bulk $FeVO_4$ mixed metal oxide contains bands at 971, 936, 910, 900, 850, 836, 773, 738, 664, 634, 370, and 327 cm^{-1} characteristic of the bulk $FeVO_4$ phase.[17] The absence of Raman bands from crystalline α-Fe_2O_3 or V_2O_5 nanophases demonstrate that the bulk $FeVO_4$ mixed metal oxide is phase pure. The dehydrated Raman spectrum of supported 4% V_2O_5/α-Fe_2O_3 catalyst is also presented in Figure 1a and is dominated by the bands of the crystalline α-Fe_2O_3 support phase. A new small band observed at ∼652 cm^{-1} is consistent with the vibrations from bridging V−O−Fe bonds. The absence of corresponding Raman bands from V_2O_5 and $FeVO_4$ nanophases indicates that these crystalline phases are not present in the supported 4% V_2O_5/α-Fe_2O_3 catalyst and suggests that the vanadium oxide phase is dispersed on the surface of α-Fe_2O_3 support as surface VO_x species. The absence of the expected V═O vibration at ∼1030 cm^{-1} in the Raman spectrum is most probably due to the strong Raman absorption by the α-Fe_2O_3 support in this region.[27]

The corresponding IR spectra of the supported V_2O_5/α-Fe_2O_3 catalyst under ambient and dehydrated conditions are presented in Figure 1b. The IR spectrum under ambient conditions exhibits two bands at ∼1600 and 970 cm^{-1}. The IR band at ∼1600 cm^{-1} is from condensed water vapor on the catalyst surface, and the band at 970 cm^{-1} arises from hydrated surface VO_x species.[5] Upon dehydration at 400 °C, the IR band from condensed water vapor is no longer present because of vaporization of the moisture, and the 970 cm^{-1} band, from the hydrated surface VO_x species, is replaced by a new sharp band at ∼1018 cm^{-1} that is characteristic of dehydrated surface VO_x species on the α-Fe_2O_3 support.[5] Thus, the IR spectra of the hydrated and dehydrated supported 4% V_2O_5 /α-Fe_2O_3 catalyst reveals that the supported vanadia phase is present as two-dimensional surface VO_x species on the α-Fe_2O_3 support.

Table 1. BET Surface Area, Total Number of Active Sites (N_s), TPSR T_p Values, and First-Order Rate Constants, k_{rds}, for HCHO Formation for Bulk α-Fe_2O_3, V_2O_5, $FeVO_4$, and Supported 4% V_2O_5/α-Fe_2O_3 Samples

catalyst	surface area (m^2/g)	N_s ($\mu mol/m^2$)	T_p (°C)	k_{rds} (s^{-1})
α-Fe_2O_3	23	7.8	186 (CH_3OH)	
			189 (HCHO)	0.19
			242 (DME)	
V_2O_5 (300)[a]	4	13.8	201	0.09
V_2O_5 (400)[b]	4	5.8		
V_2O_5 (450)[2]	4	0.7		
$FeVO_4$	8	3.1	200	0.09
supported 4% V_2O_5/α-Fe_2O_3	23	3.8	195	0.13

[a] The number given in the bracket is the temperature in °C at which NH_4VO_3 was calcined for 4 h to obtain the V_2O_5 bulk oxide. [b] Ref 11. [2] Ref 14.

3.3. High-Resolution Transmission Electron Microscopy (HR-TEM). *3.3.1. Bulk $FeVO_4$ Catalyst.* Representative BF and HR-TEM images of the bulk $FeVO_4$ material are presented in Figure 2a and b, respectively. A bimodal distribution of particle sizes was observed in the BF image of the $FeVO_4$ sample in Figure 2a with the majority of the particles in the 100−200 nm size range and the minority in the 10−50 nm size range. Regardless of particle size, an amorphous surface overlayer was always observed having a thickness of 0.4−2.0 nm. The amorphous overlayer is clearly visible in profile view in Figure 2b and is

dx.doi.org/10.1021/cs1000569 |ACS Catal. 2011, 1, 54–66

consistent with previous observations of Luo et al.[28,29] Similar amorphous overlayers have also been previously observed in other bulk mixed oxide catalyst systems.[30−32] It was proposed that the amorphous overlayer was a thermodynamic equilibrium structure[29] and the variations in the amorphous layer thickness could be a result of different crystal facet terminations or local fluctuations in calcination conditions. It should be noted, however, that such mixed oxide materials are often prone to electron beam damage,[33] and structural modification can sometimes be observed under prolonged intense electron irradiation. Although experimental conditions were carefully optimized during our HR-TEM image acquisition to minimize damage to the sample, we cannot rule out the possibility that some small fraction of the observed amorphous layer may be a result of electron-beam-induced amorphization. Analysis of the lattice fringe details in our HR-TEM images confirms that the bulk $FeVO_4$ phase adopts a triclinic structure.

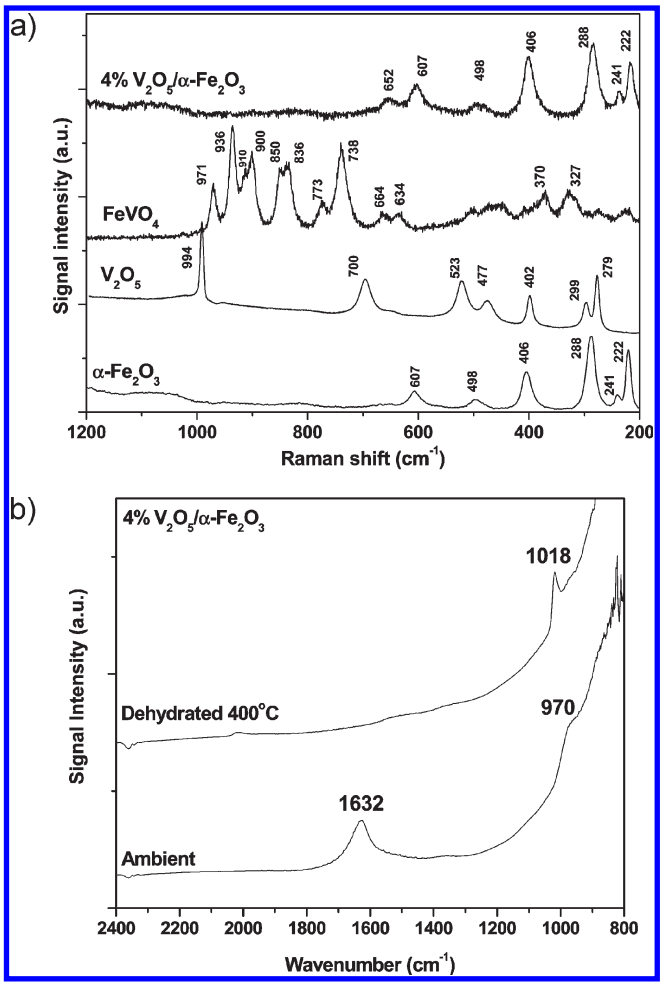

Figure 1. (a) Raman spectra of bulk α-Fe_2O_3 (dehydrated), V_2O_5 (ambient), $FeVO_4$ (ambient), and supported 4% V_2O_5/α-Fe_2O_3 (dehydrated) catalysts. (b) IR spectra of the supported 4% V_2O_5/α-Fe_2O_3 catalyst under ambient and dehydrated conditions at room temperature.

Elemental analysis by electron energy loss spectroscopy (EELS) analysis was performed using an electron probe having a 1 Å FWHM size and 15 pA probe current. To reduce beam damage effects, the electron probe was rastered over a 2×2 nm^2 area at high scanning speed during EELS spectral acquisition. An EELS spectrum was acquired from both the center and the edge of individual $FeVO_4$ particles (Figure 3). Although some loss of material and reduction of V^{5+} and Fe^{3+} (as revealed by the changes in the electron energy-loss near-edge structure) under the electron beam was observed during EELS spectra acquisition, preferential sputtering of V or Fe atoms should not be an issue since they have very similar atomic masses. Qualitative analysis of the EELS spectra (using the V $L_{2,3}$ and Fe $L_{2,3}$ edges) revealed a definite increase in V/Fe ratio at the edge of the catalyst particles, 1.1 ± 0.1 at the center and 1.5 ± 0.2 at the edge, reflecting that V is enriched, relative to Fe, in the surface layers of the catalyst.

3.3.2. Model-Supported 4% V_2O_5/α-Fe_2O_3 Catalyst. Representative BF and HR-TEM images of the 4% V_2O_5/α-Fe_2O_3 model catalyst are presented in Figure 4a and b, respectively. A broad particle size distribution ranging from 10 to 100 nm was observed for this sample, and most of the particles possessed a faceted plate-like morphology (Figure 4a). No discrete crystalline V_2O_5 or $FeVO_4$ phases were found by selected area electron diffraction (SAED), which matches well with a pure α-Fe_2O_3 phase (See Figure S1, Supporting Information). Even though the HR-TEM images of this model catalyst were taken under identical low dose illumination conditions to those used for the $FeVO_4$ sample, no obvious amorphous layers were observed in

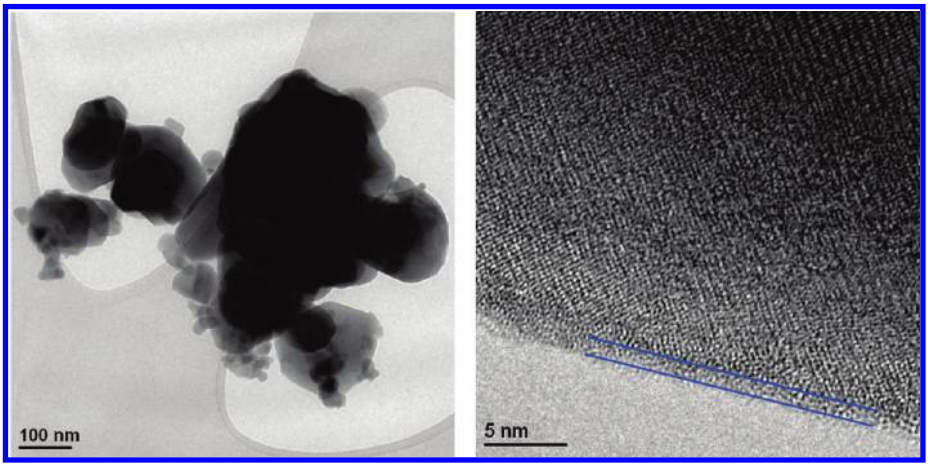

Figure 2. (a) Representative BF-TEM image of the $FeVO_4$ catalyst. (b) Representative HR-TEM image of a triclinic $FeVO_4$ particle along the $[\bar{1}22]$ zone axis in which a surface amorphous layer is evident.

dx.doi.org/10.1021/cs1000569 |*ACS Catal.* 2011, 1, 54–66

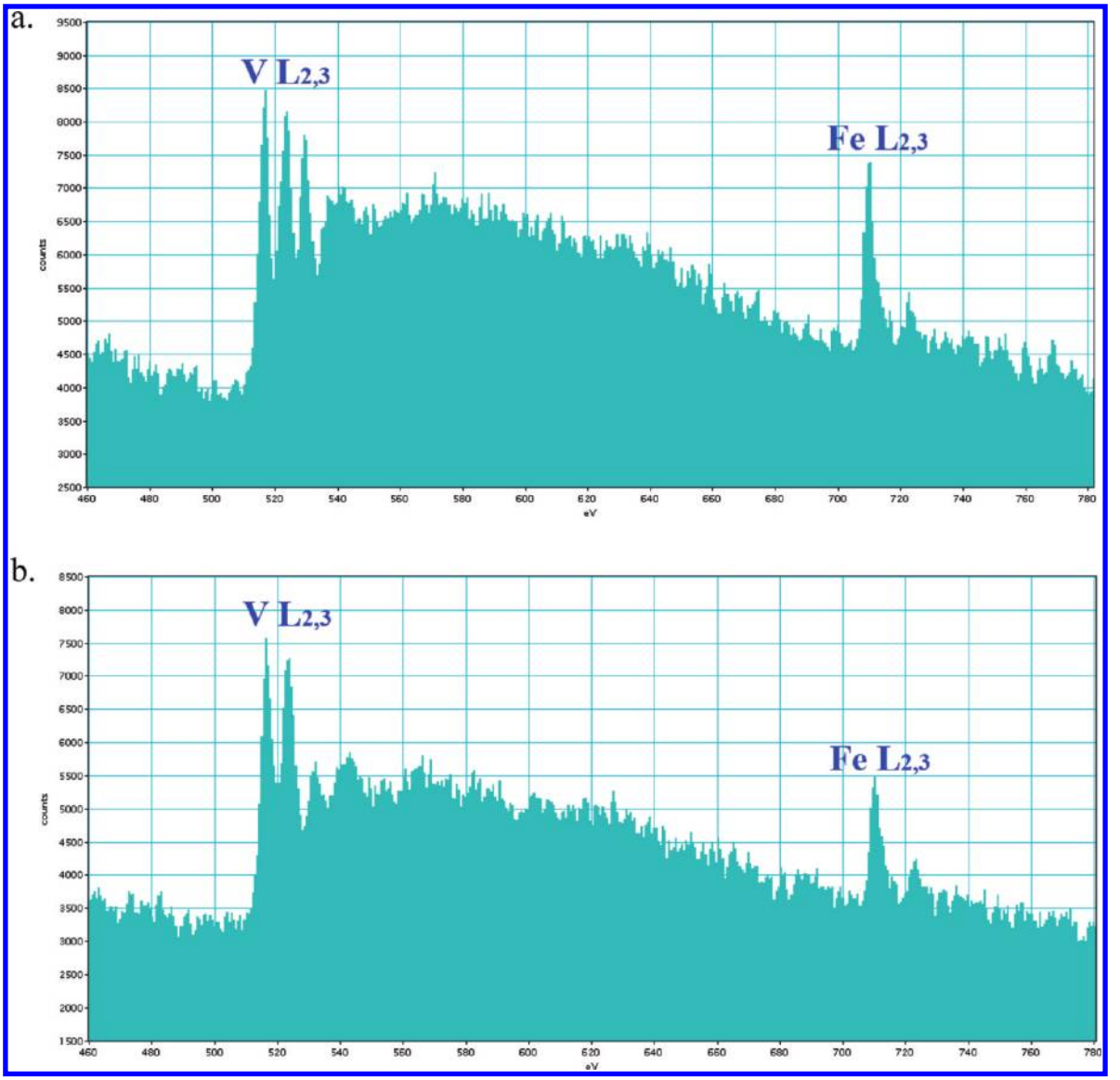

Figure 3. EELS spectra taken from (a) the center and (b) the edge of a bulk $FeVO_4$ catalyst particle using a 1 Å probe scanned in a 2 × 2 nm^2 raster. The V/Fe atomic ratios are 1.1 ± 0.1 in spectrum a and 1.5 ± 0.2 in spectrum b.

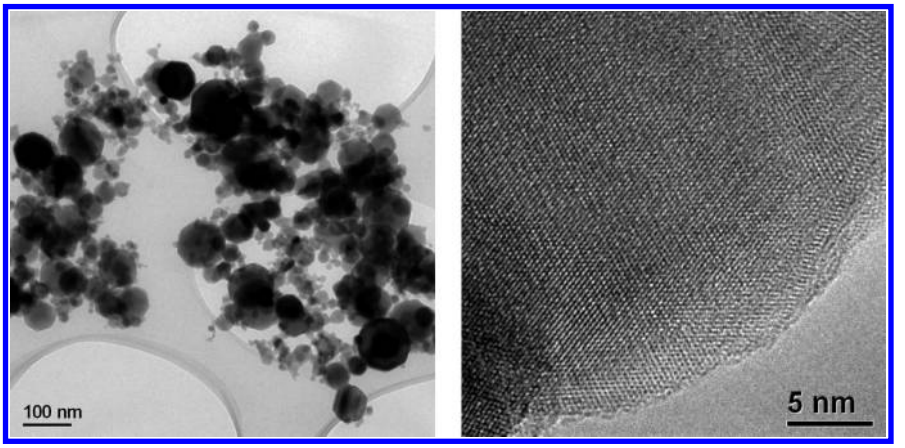

Figure 4. (a) Representative BF-TEM micrograph of the model supported 4% V_2O_5/α-Fe_2O_3 catalyst. (b) Representative HR-TEM micrograph of the model supported 4% V_2O_5/α-Fe_2O_3 catalyst.

dx.doi.org/10.1021/cs1000569 |*ACS Catal.* 2011, 1, 54–66

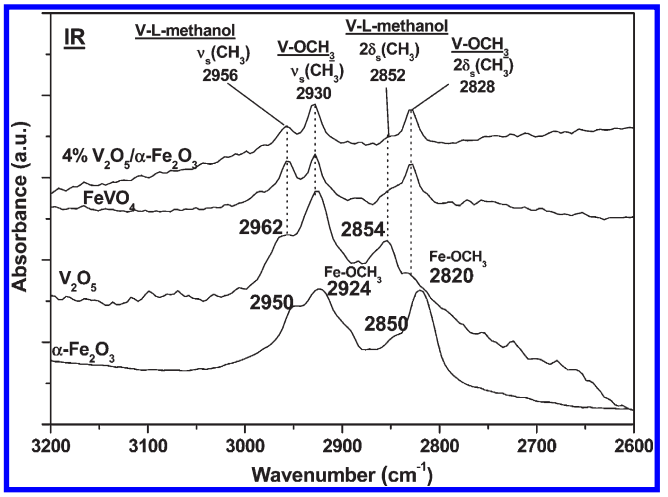

Figure 5. Methanol-infrared spectra of bulk α-Fe_2O_3, V_2O_5, $FeVO_4$, and supported 4% V_2O_5/α-Fe_2O_3 catalysts after CH_3OH chemisorption at 100 °C.

this model catalyst material (Figure 4b). This suggests that the supported vanadium oxide phase is well dispersed in a monolayer or submonolayer fashion on the surface of the crystalline α-Fe_2O_3 particles. The presence of the dispersed VO_x over the α-Fe_2O_3 particle surface was confirmed by the weak V signal in both X-ray energy dispersive spectra (XEDS) and EELS spectra collected from this sample.

3.4. CH_3OH-IR Spectroscopy. The in situ IR spectra after methanol chemisorption at 100 °C on the bulk V_2O_5, α-Fe_2O_3, $FeVO_4$, and supported 4% V_2O_5/α-Fe_2O_3 catalysts are presented in Figure 5. The IR spectra prior to the CH_3OH adsorption on the dehydrated catalyst sample in the O_2/He environment have been subtracted from that of methanol-exposed surfaces to isolate the surface vibrations resulting from methanol adsorption. Both surface CH_3O^* and intact surface CH_3OH^* species, with the molecular methanol bound to Lewis acid surface sites ($L-CH_3OH$), are observed for the bulk α-Fe_2O_3, V_2O_5, $FeVO_4$, and supported 4% V_2O_5/α-Fe_2O_3 catalysts. For all samples, the presence of surface CH_3O^* species is prominent compared to the surface intact CH_3OH^* species. For bulk α-Fe_2O_3, the surface $Fe-OCH_3$ vibrations are observed at 2924 and 2820 cm^{-1}, whereas the surface $Fe-CH_3OH$ vibrations appear at 2950 and 2850 cm^{-1}. Methanol chemisorption on bulk V_2O_5 gives rise to a sharp peak at 2930 cm^{-1} and a broad band at 2828 cm^{-1}, which are assigned to the vibrations of surface $V-OCH_3$ species, the bands at 2962 and 2854 cm^{-1} originate from the intact surface $V-CH_3OH$ species. For bulk $FeVO_4$, predominantly surface CH_3O^* species are observed at 2930 and 2828 cm^{-1}, along with a smaller signal for the intact surface CH_3OH^* species at 2956 and 2852 cm^{-1}. The surface CH_3O^* vibrations on $FeVO_4$ match the vibrations of the surface $V-OCH_3$ indicating that bulk $FeVO_4$ phase is surface enriched with VO_x species. The surface CH_3O^* (2930 and 2828 cm^{-1}) and CH_3OH^* (2956 and 2852 cm^{-1}) vibrations from the supported 4% V_2O_5/α-Fe_2O_3 catalyst also match the vibrations of surface $V-OCH_3$ and $V-CH_3OH$ indicating that the α-Fe_2O_3 support is covered by approximately a monolayer of surface VO_x species. Comparison of the CH_3OH-IR spectrum of bulk $FeVO_4$ with the IR spectrum of monolayer supported V_2O_5/α-Fe_2O_3 reveals that the bulk $FeVO_4$ catalyst also possesses approximately monolayer surface VO_x coverage.

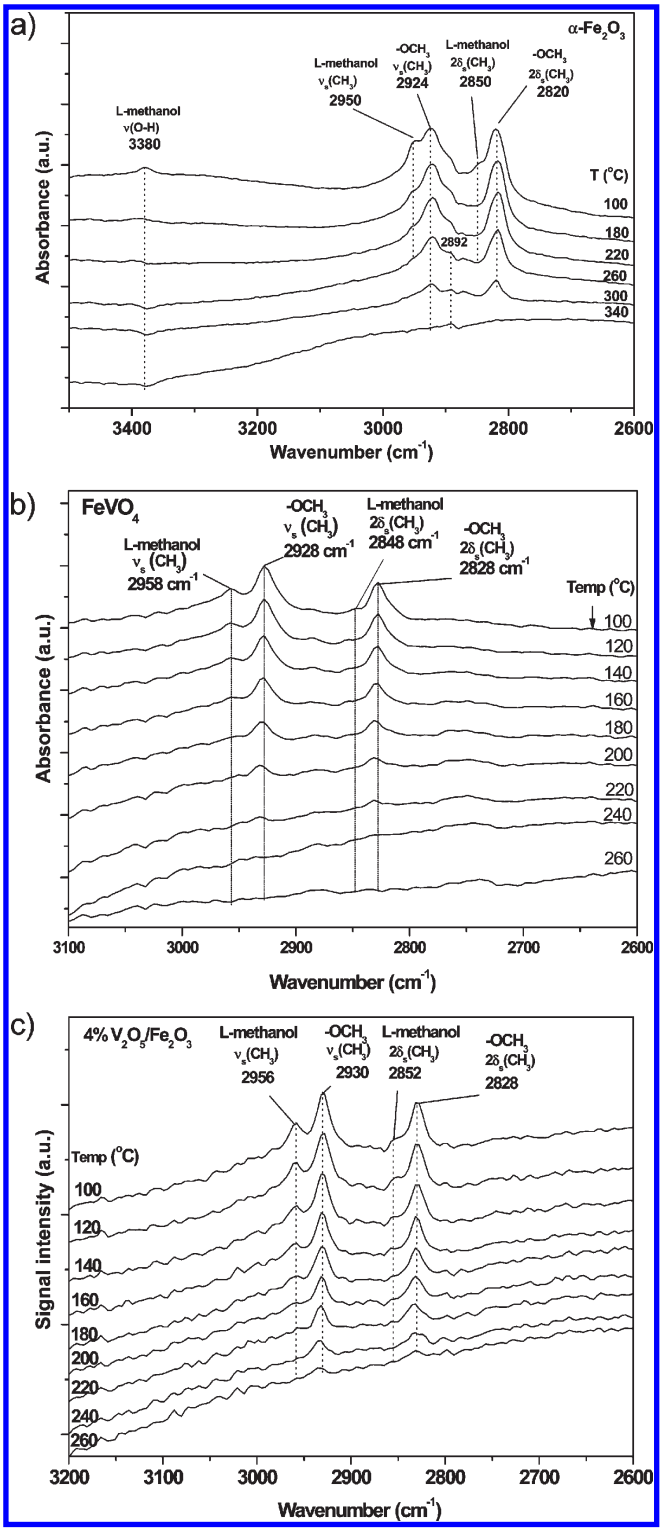

Figure 6. (a) Temperature-programmed CH_3OH-IR spectra from the α-Fe_2O_3 support. (b) Temperature-programmed CH_3OH-IR spectra from the bulk $FeVO_4$ catalyst. (c) Temperature-programmed CH_3OH-IR from the supported 4% V_2O_5/α-Fe_2O_3 catalyst.

The CH_3OH-temperature-programmed IR (TPIR) spectra for the catalysts are presented in Figure 6a−c and reveal the surface reactivity of intact surface CH_3OH^* and surface CH_3O^* species on the different catalytic materials.

dx.doi.org/10.1021/cs1000569 |*ACS Catal.* 2011, 1, 54–66

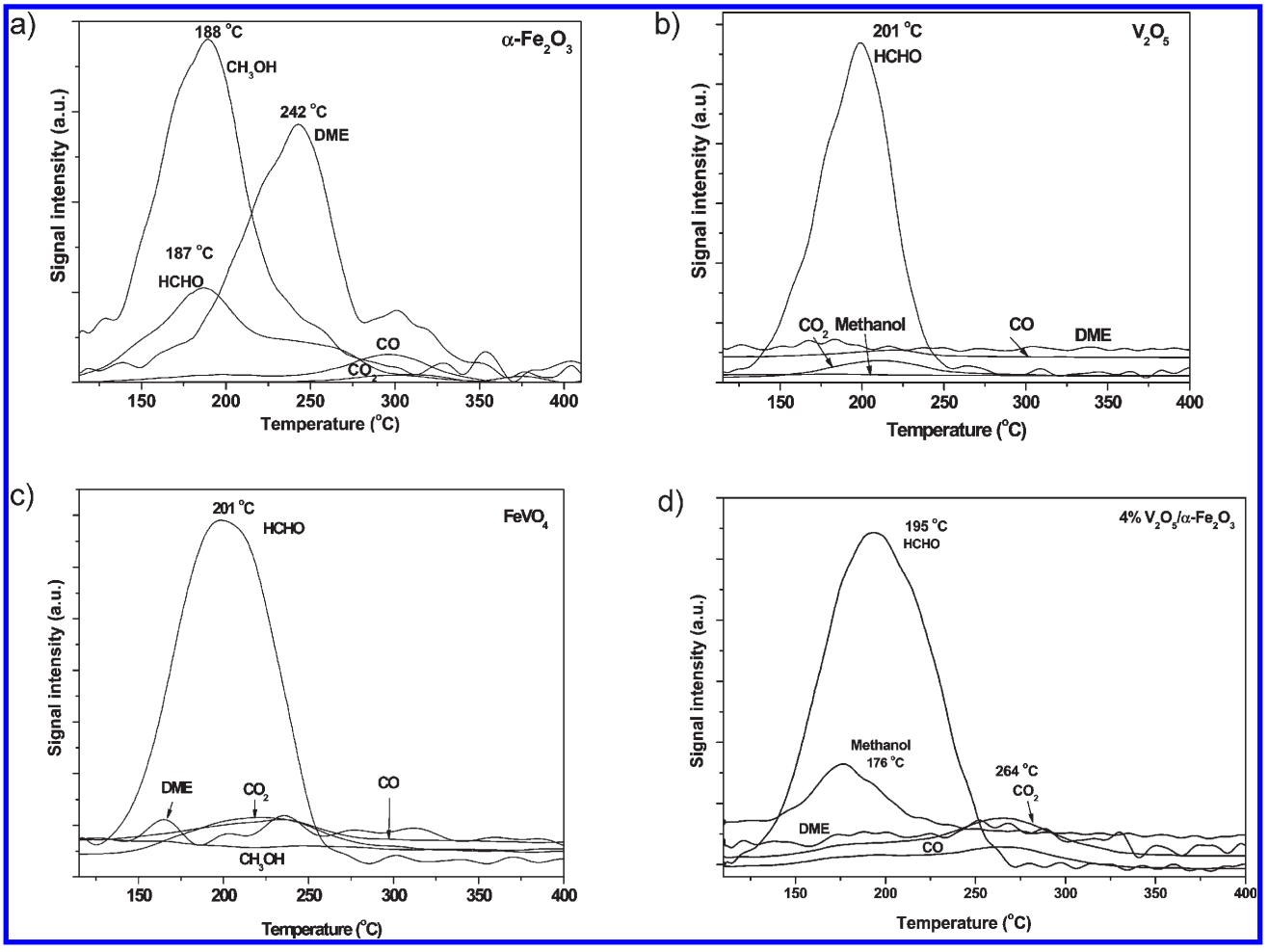

Figure 7. (a) CH_3OH-TPSR spectra from the α-Fe_2O_3 support catalyst. (b) CH_3OH-TPSR spectra from the bulk V_2O_5 catalyst. (c) CH_3OH-TPSR spectra from the bulk $FeVO_4$ catalyst. (d) CH_3OH-TPSR spectra from the supported 4% V_2O_5/α-Fe_2O_3 catalyst.

3.4.1. Bulk α-Fe_2O_3. The CH_3OH-temperature programmed IR spectra from α-Fe_2O_3 are illustrated in Figure 6a. The IR bands at 2950 and 2850 cm^{-1} of the intact surface Fe−CH_3OH species are observed and decrease with increasing temperature and completely disappear at ∼260 °C. The intact surface methanol O−H vibration ν(O−H) at 3380 cm^{-1} also completely disappears by ∼260 °C. The disappearance of chemisorbed intact Fe−CH_3OH from the α-Fe_2O_3 surface during CH_3OH-TPIR corresponds to the appearance of CH_3OH in the gas phase during CH_3OH-TPSR (see Figure 7a below), which indicates that the intact surface Fe−CH_3OH species is responsible for the appearance of CH_3OH in the gas phase in this temperature range.

The IR bands for the surface Fe−OCH_3 species (2924 and 2820 cm^{-1}), however, only completely disappear above 300 °C and reflect their lower surface reactivity on α-Fe_2O_3 than the intact surface Fe−CH_3OH. The temperature range where the surface methoxy intermediate reacts corresponds to the appearance of gas phase DME during the CH_3OH-TPSR experiment (see Figure 7a). Thus, the surface Fe-OCH_3 species on α-Fe_2O_3 are responsible for the formation of DME.

3.4.2. Bulk V_2O_5. For bulk V_2O_5, methanol chemisorption also results in the appearance of IR bands for both intact surface V−CH_3OH (2962 and 2854 cm^{-1}) and surface V−OCH_3 (2930 and 2828 cm^{-1}) species, with the latter predominating as shown in Figure 5. The CH_3OH-TPIR experiment, unfortunately, did not result in good quality IR spectra because of the quite low surface area of the V_2O_5 sample and the preferential chemisorption of methanol only on the edge planes.[34] Thus, the CH_3OH-TPIR spectra for V_2O_5 are not presented. The bulk V_2O_5 catalyst, however, exclusively yields HCHO from redox sites and no DME from acid sites during CH_3OH-TPSR (see Figure 7b below).

3.4.3. Bulk $FeVO_4$. The CH_3OH-TPIR spectra from the bulk $FeVO_4$ catalyst are shown in Figure 6b. As the temperature is increased, the IR bands of the intact V−CH_3OH species (∼ 2958 and 2852 cm^{-1}) decrease and disappear at ∼180 °C. The same trend is also observed for the surface V−CH_3O species (2928 and 2828 cm^{-1}) that decrease with temperature and completely disappear at ∼260 °C. Comparison of the CH_3OH-TPIR findings with the corresponding CH_3OH-TPSR spectra from bulk $FeVO_4$ reveal that both species give rise to HCHO production from redox sites since DME is not formed (see Figure 7c).

3.4.4. Supported 4% V_2O_5/α-Fe_2O_3. The CH_3OH-TPIR spectra from the supported 4% V_2O_5/α-Fe_2O_3 catalyst are presented in Figure 6c and exhibit the presence of the intact surface V−CH_3OH (2956 and 2852 cm^{-1}) and surface V−OCH_3 (2930 and 2828 cm^{-1}) species, with the latter being the predominant species. With increasing temperature, both surface intermediate species react and desorb from the surface

dx.doi.org/10.1021/cs1000569 |*ACS Catal.* 2011, 1, 54–66

at ~260 °C and form HCHO (see Figure 7d), which reflects the presence of surface redox sites for the supported 4% V_2O_5/α-Fe_2O_3 catalyst. Thus, the exclusive formation of HCHO and the absence of DME from the supported 4% V_2O_5/α-Fe_2O_3 catalyst further reveal that the acidic FeO_x sites are covered by the surface VO_x monolayer.

3.5. CH_3OH-Temperature Programmed Surface Reaction Spectroscopy. The TPSR spectroscopy experiments were performed with CH_3OH as the probe molecule to study the surface chemical properties of the metal oxide catalysts. As already shown above, both intact surface CH_3OH^* and CH_3O^* intermediates are formed upon methanol exposure to the metal oxide catalysts being investigated in this study. Depending on the nature of active sites, the surface intermediate yields HCHO from redox sites, CH_3OCH_3 from acid sites, and CO/CO_2 from basic sites.[16] In addition, CO/CO_2 can also be formed from overoxidation of HCHO, which must be minimized. The number of each type of catalytic active site can also be determined from the area under each TPSR spectrum (HCHO, CH_3OCH_3, or CH_3OH). In addition, the maximum peak temperature is also used to calculate the rate constant, k_{rds}, for the rate-determining-step of the surface reaction.

The CH_3OH-TPSR spectra for the bulk α-Fe_2O_3, V_2O_5, $FeVO_4$, and supported 4% V_2O_5/α-Fe_2O_3 catalysts are shown in Figure 7a−d.

3.5.1. Bulk α-Fe_2O_3. The CH_3OH-TPSR spectra from α-Fe_2O_3 are presented in Figure 7a. The primary reaction product is DME with a T_p value of ~242 °C. A significant amount of CH_3OH also appears with a $T_p \approx 188$ °C, reflecting the inactivity of many of the surface sites. In addition, small amounts of HCHO desorbs with a $T_p \approx 187$ °C, as well as CO/CO_2 with a $T_p \approx 300$ °C. The absence of any significant HCHO and CO/CO_2 formation indicates the minor concentration of surface redox and basic sites on the acidic α-Fe_2O_3 surface.

3.5.2. Bulk V_2O_5. The CH_3OH-TPSR spectra from bulk V_2O_5 are presented in Figure 7b. The primary reaction product from bulk V_2O_5 is HCHO with a T_p value of ~201 °C. The almost complete absence of CH_3OH desorption suggests that all the surface sites are active for methanol oxidation. The absence of any significant DME from acid sites and CO/CO_2 from basic sites indicate that the surface of V_2O_5 mainly consists of redox sites.

3.5.3. Bulk $FeVO_4$. The CH_3OH-TPSR spectra from bulk $FeVO_4$ are presented in Figure 7c. The primary product is HCHO, which desorbs with a T_p value of ~195 °C. The complete absence of CH_3OH desorption reveals that essentially all the surface sites are reactive. The minor amounts of DME and CO/CO_2 formation reflect the surface redox nature of the bulk $FeVO_4$ catalyst. Comparison of the CH_3OH-TPSR results for bulk V_2O_5, α-Fe_2O_3, and $FeVO_4$ reveals that the surface chemistry of $FeVO_4$ is dominated by that of redox surface vanadium oxide sites and not the acidic surface iron oxide sites.

3.5.4. Supported V_2O_5/α-Fe_2O_3. The CH_3OH-TPSR spectra for the supported 4% V_2O_5/α-Fe_2O_3 catalyst are shown in Figure 7d. Similar to the other V-containing catalysts, only HCHO is produced from surface redox sites. The absence of any DME formation reveals that the surface acidic sites of α-Fe_2O_3 are extensively covered by the redox surface VO_x sites. The minor amounts of CO and CO_2 also reflect the absence of significant surface basic sites. The HCHO T_p value is ~200 °C, which is identical to that of bulk $FeVO_4$ and V_2O_5 catalysts. This suggests that similar catalytic active surface redox sites are present for the model-supported 4% V_2O_5/α-Fe_2O_3 and bulk $FeVO_4$ catalysts.

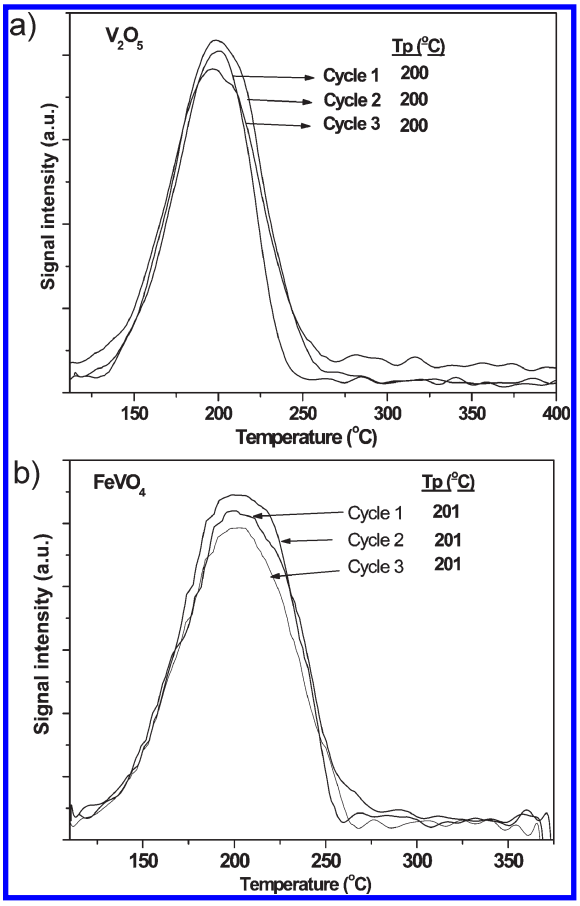

Figure 8. (a) Cyclic HCHO/CH_3OH-TPSR spectra from the bulk V_2O_5 catalyst (the catalyst was not oxidized between the TPSR experiments). (b) Cyclic HCHO/CH_3OH-TPSR spectra from the bulk $FeVO_4$ catalyst (the catalyst was not oxidized between the TPSR experiments).

3.6. Cyclic CH_3OH-TPSR Experiments. To obtain additional insights into the mechanism of the selective oxidation of methanol to formaldehyde over the bulk V_2O_5 and $FeVO_4$ catalysts, cyclic HCHO/CH_3OH-TPSR experiments were performed in the absence of gas phase oxygen. The reducing cyclic HCHO/CH_3OH-TPSR experiments, where the V_2O_5 and $FeVO_4$ catalysts were not oxidized between each CH_3OH-TPSR experiment, are presented in the Figure 8a and b, respectively. Note that the HCHO T_p value, as well as the total amount of HCHO produced, remains essentially the same as the bulk mixed metal oxide is progressively reduced by CH_3OH in each TPSR cycle. The constant T_p value for the HCHO/CH_3OH-TPSR experiments indicates that the oxidation state of surface VO_x sites does not change with the cyclic CH_3OH-TPSR experiments.[35] The almost constant HCHO production also indicates that the number of surface catalytic active sites remains the same with each reducing CH_3OH-TPSR cycle. This suggests that the diffusion of lattice oxygen from the bulk to surface is a relatively fast process, certainly when compared to steady-state oxidation that is conducted at much higher reaction temperatures and is able to reoxidize all the reduced surface VO_x species of the bulk $FeVO_4$ catalyst. Essentially the same behavior is found for bulk V_2O_5 and supported 4% V_2O_5/α-Fe_2O_3 catalysts (not shown for brevity). Thus, both bulk $FeVO_4$ and V_2O_5 catalysts operate by the Mars−van Krevelen mechanism during methanol oxidation

dx.doi.org/10.1021/cs1000569 |ACS Catal. 2011, 1, 54–66

Table 2. Catalytic Behavior of Oxide Catalysts during Steady-State Selective Oxidation of Methanol at 230 °C (CH_3OH/O_2/He = 6:13:81; Total Flow Rate = 100 cm^3 m^{-1})

	selectivity (%)					
catalyst	HCHO	DME	DMM	overall rate (μmol m^{-2} s^{-1})	TOF_{Redox} (s^{-1})	K_{ads} (atm^{-1})
α-Fe_2O_3	0	70	30	0.7	0.07*	
V_2O_5	87	0	13	1.2	0.08	15
$FeVO_4$	83	0	17	0.62	0.16	28
supported 4% V_2O_5/α-Fe_2O_3	78	7	15	0.38	0.10	13

* Estimated from 30% DMM selectivity where DMM formation involves one HCHO and two surface CH_3O^* intermediates.

to formaldehyde with the supply of bulk lattice oxygen being a very rapid kinetic process.[36]

3.7. N_s (Number of Catalytic Active Sites (μmol m^{-2})). The number of exposed catalytic active sites for the bulk and supported metal oxide catalysts was determined by integrating the HCHO/CH_3OH-TPSR and DME/CH_3OH-TPSR spectra since they represent the number of surface redox and acid sites, respectively, and are listed in Table 1, where the values are normalized per unit surface area. The number of catalytic active sites for crystalline bulk α-Fe_2O_3 was found to be 7.8 μmol m^{-2}.[16] The surface density of the number of sites for the supported 4% V_2O_5/α-Fe_2O_3 catalyst is 3.8 μmol m^{-2} indicating that there is ~50% fewer sites when the surface VO_x monolayer is deposited on the α-Fe_2O_3 support. The surface sites on the supported V_2O_5/α-Fe_2O_3 catalyst, however, are redox in nature whereas the surface sites on α-Fe_2O_3 tend to be acidic. The number of catalytic active sites for bulk V_2O_5 is dependent on calcination temperature and significantly decreases with calcination temperature (13.8, 5.8, and 0.7 μmol m^{-2} for calcination at 300, 400, and 450 °C, respectively). The calcination temperature variation in N_s is related to the crystallization of the V_2O_5 phase where the fully crystallized V_2O_5 possesses platelet morphology with methanol only chemisorbing on the edge planes of this anisotropic phase.[13,16] Bulk $FeVO_4$ crystallizes in an isotropic morphology and contains 3.1 μmol m^{-2} of surface redox sites, which is greater than that found on the anisotropic V_2O_5 crystalline platelets calcined at the same temperature. Thus, the surface density of the number of catalytic active sites for methanol oxidation is a factor of ~4 greater for bulk $FeVO_4$ than V_2O_5 because of their different crystalline morphology. Furthermore, the surface density of redox catalytic active sites on both bulk $FeVO_4$ and the monolayer supported V_2O_5/α-Fe_2O_3 catalyst are almost identical and is consistent with the presence of a surface VO_x monolayer on the bulk $FeVO_4$ phase.

3.8. First-Order Rate Constant (k_{rds}) for HCHO Formation. The first-order rate constants for HCHO formation from oxidation of the surface CH_3O^* and CH_3OH^* intermediates were determined by application of the Redhead equation using the CH_3OH-TPSR T_p values and are listed in Table 1 and indicate that the V-containing catalysts exhibit comparable redox activity toward HCHO formation. Although the bulk α-Fe_2O_3 support catalyst possesses slightly more active redox sites than the V-containing catalysts, the number of redox sites present on the predominantly acidic α-Fe_2O_3 is a minor amount.

3.9. Steady-State Methanol Oxidation. Methanol oxidation was investigated over the bulk and supported catalysts under steady-state conditions at 230 °C and the resulting catalytic activity and selectivity are presented in Table 2. Note that only traces of CO and CO_2 were formed as reaction products indicating that basic surface sites represent only a minor number of catalytic active sites during steady-state methanol oxidation on these catalysts. The turnover frequency (TOF) values are defined as the rates of reaction per active site per second and are also presented in Table 2. The number of catalytic active sites, N_s, was obtained from the CH_3OH-TPSR experiments, contained in Table 1 and was employed in calculating the TOF values. The TOF_{redox} values were determined by multiplying the overall TOF with the steady-state HCHO selectivity.

3.9.1. Bulk α-Fe_2O_3. The bulk α-Fe_2O_3 catalyst is highly selective toward DME formation, which reflects the acidic nature of the surface FeO_x sites. Dimethoxy methane (DMM) formation requires the presence of redox sites to produce HCHO that subsequently reacts with CH_3OH on acid sites to form DMM.[37] The formation of some DMM indicates that surface redox sites are also present on the α-Fe_2O_3 catalyst (estimated as 10% or ~0.8 μmol/m^2 since DMM formation requires one HCHO and two surface CH_3O^* intermediates and DMM selectivity is 30). At higher temperatures, HCHO formation from surface redox sites becomes more pronounced. Thus, the surface FeO_x sites of bulk α-Fe_2O_3 exhibit both surface acidic and redox sites during methanol oxidation, with the acidic sites being dominant. The overall rate of methanol oxidation at 230 °C for bulk α-Fe_2O_3 is calculated to be 0.7 μmol/m^2-s and the TOF_{redox} is estimated as 0.07 s^{-1}.

3.9.2. Bulk V_2O_5. The bulk V_2O_5 catalyst primarily contains surface redox sites during methanol oxidation as reflected in the high selectivity toward HCHO production. A minor amount of surface acid sites are also present during steady-state methanol oxidation since the small amount of DMM formation requires the presence of surface acid sites.[37] The surface area normalized overall activity, μmol m^{-2} s^{-1}, for the bulk V_2O_5 catalyst is within a factor of 2 of the overall activity for the bulk α-Fe_2O_3 catalyst indicating that vanadium oxide redox sites have comparable activity to the iron oxide acid sites (see Table 2) for methanol conversion. The TOF_{redox} values for bulk V_2O_5 and the redox sites present for bulk α-Fe_2O_3 are also comparable for methanol oxidation (see Table 2). Thus, bulk V_2O_5 predominantly contains very active surface redox sites with a minor amount of surface acid sites and the normalized activity of bulk V_2O_5 comparable to the catalytic active sites present for bulk α-Fe_2O_3.

3.9.3. Bulk $FeVO_4$. For the stoichiometric, bulk $FeVO_4$ mixed metal oxide catalyst, the HCHO selectivity is 83% reflecting the redox nature of its catalytic surface. The minor formation of DMM reveals that some surface acid sites are also present for the bulk $FeVO_4$ catalyst (estimated as ~12% from the DMM selectivity). The selectivity toward HCHO and DMM, as well as surface area normalized overall activity are very close to that

dx.doi.org/10.1021/cs1000569 |ACS Catal. 2011, 1, 54–66

found for bulk V_2O_5 as indicated in Table 2. The similar catalytic performance of bulk V_2O_5 and $FeVO_4$ suggests that the surface VO_x sites are the catalytic active sites for the bulk $FeVO_4$ mixed metal oxide catalyst for methanol oxidation to formaldehyde.

3.9.4. Supported 4% V_2O_5/α-Fe_2O_3. The presence of the dispersed surface VO_x species on the α-Fe_2O_3 support for the supported V_2O_5/α-Fe_2O_3 catalyst dramatically alters the surface nature of the supported V_2O_5/α-Fe_2O_3 catalyst compared to that of the bulk α-Fe_2O_3 support catalyst as indicated in Table 2. The presence of the surface VO_x species converts the predominantly acidic α-Fe_2O_3 surface (70% DME, 30% DMM and 0% HCHO) to a predominantly redox surface (78% HCHO, 15% DMM, and 7% DME). The formation of the minor amount of DME may be related to residual exposed surface FeO_x sites. Note that the catalytic performance of the supported V_2O_5/α-Fe_2O_3 and bulk $FeVO_4$ catalysts are almost identical indicating that it is the surface VO_x sites on the bulk $FeVO_4$ catalyst that are the catalytic active sites for methanol oxidation to formaldehyde.

4. DISCUSSION

4.1. Bulk Structure of $FeVO_4$. The crystalline $FeVO_4$ possess a triclinic structure, belonging to the $P\bar{1}$ space group and consists of three distinct isolated VO_4 units.[12,38] The triplet of bands at 971 and 936 cm^{-1} and a third weak band at ~900 cm^{-1} were assigned to the short V═O bond stretching of each of the three VO_4 units.[38] The vibrations at ~910 and ~900, ~ 850 and ~834, and 773 and 738 cm^{-1} were assigned to the asymmetric stretches of the three isolated VO_4 sites. The Raman bands at ~370 and ~327 cm^{-1} belong to the associated VO_4 asymmetric and symmetric bending vibrations, respectively. The asymmetric stretching vibrations at 663 and 634 cm^{-1}, symmetric stretching at 500 and 460 cm^{-1}, and weak bending modes at 200−300 cm^{-1} have been assigned to the bridging V−O−Fe bonds present in the bulk $FeVO_4$ crystalline structure.[12]

In situ Raman spectroscopy is the technique of choice for characterization of bulk mixed metal oxide catalysts, especially bulk $FeVO_4$, under reaction conditions since Raman can discriminate between all three distinct VO_4 units in bulk $FeVO_4$, while other in situ characterization methods just signal average over the three VO_4 units (e.g., XANES/EXAFS). In situ Raman spectroscopy of bulk mixed metal oxides functioning with the Mars−van Krevelen mechanism have demonstrated that bulk mixed oxide catalysts are essentially the same under oxidizing (O_2/He) and reaction conditions ($O_2/CH_3OH \gg 2$).[41] This observation is consistent with the first-order partial pressure dependence of methanol, since the rate-determining-step involves dehydrogenation of surface methoxy to formaldehyde, and the zero-order dependence in oxygen partial pressure.

4.2. Surface Composition of $FeVO_4$. The bulk $FeVO_4$ phase is surface enriched with VO_x species. This is reflected in the CH_3OH-IR spectrum from $FeVO_4$ that is almost indistinguishable from the monolayer supported 4% V_2O_5/α-Fe_2O_3 catalyst demonstrating the predominance of surface V−OCH_3 and V−CH_3OH intermediates. The absence of distinct Fe−OCH_3 and Fe−CH_3OH IR vibrations for both bulk $FeVO_4$ and supported V_2O_5/α-Fe_2O_3 catalysts confirms that the concentration of exposed surface FeO_x sites is low in these catalysts. This is further reflected by the absence of acidic reaction products during CH_3OH-TPSR and only a minor amount of DMM and DME during steady-state methanol oxidation. The surface enriched VO_x layer on bulk $FeVO_4$ is consistent with the increase of V/Fe atomic ratio in the surface region of the $FeVO_4$ particles as revealed by STEM-EELS analysis. Moreover, a thin amorphous surface layer is always observed on the $FeVO_4$ particle in our HR-TEM images, suggesting that this thin amorphous layer on the bulk $FeVO_4$ catalyst may well contain an amorphous overlayer of surface VO_x species that approaches monolayer coverage. It was not possible to independently determine the composition of the outermost surface layer for $FeVO_4$ with low energy ion scattering (LEIS) spectroscopy because the atomic numbers for V and Fe are too close to obtain separate He^+ LEIS signals from the two different surface sites.

The enriched surface VO_x sites on the $FeVO_4$ mixed metal oxide is related to the high mobility of the V^{5+} cation and the driving force to decrease the surface free energy of the mixed metal oxide system.[35] Surface VO_x sites tend to terminate in V═O bonds, while surface FeO_x sites tend to terminate in Fe−OH bonds, and the surface free energy of terminating M═O surfaces, such as in bulk V_2O_5, are much lower than terminating M−OH surfaces.[39] The enhanced mobility of VO_x is associated with its much lower Tammann temperature, defined as half the melting point, of V_2O_5 (209 °C) compared to α-Fe_2O_3 (646 °C).[40] The Tammann temperature represents the temperature that surface atoms of a material begin to diffuse and suggest that the mobility of VO_x is significantly greater than that for FeO_x. Thus, the much higher mobility and lower surface free energy of VO_x relative to FeO_x is responsible for the surface VO_x enrichment of the bulk $FeVO_4$ mixed metal oxide phase.

4.3. Surface Structure of $FeVO_4$. The strong Raman bands from crystalline $FeVO_4$ prevent detection of a Raman signal from the weakly scattering surface region of bulk $FeVO_4$.[12] The only surface structural information about iron vanadia systems comes from the IR spectrum of the dehydrated model supported 4% V_2O_5/α-Fe_2O_3 catalyst that possess a two-dimensional surface VO_x monolayer (see Figure 1b). The IR band position for the dehydrated surface VO_x species at 1018 cm^{-1} is only consistent with a mono-oxo V═O surface O═VO_3 species that has three bridging V−O−Fe or V−O−V bonds as for other supported vanadia catalysts.[5]

4.4. Number Density and Nature of Catalytic Active Sites of $FeVO_4$. The interaction of vanadium oxide and iron oxide affects both the number density and nature of the catalytic active sites. Crystalline V_2O_5 contains few catalytic active sites on the edge of the anisotropic platelet morphology that possess redox character. Crystalline α-Fe_2O_3 contains an order of magnitude greater number of catalytic active sites because all the exposed planes of this isotropic phase are capable of chemisorbing methanol, but the surface sites are predominantly acidic in nature. The solid state reaction between anisotropic V_2O_5 and isotropic α-Fe_2O_3 to form isotropic $FeVO_4$ yields a catalytic material in which the number of redox catalytic active sites significantly increases from 0.7 μmol m^{-2} s^{-1} for V_2O_5 to 3.1 μmol m^{-2} s^{-1} for $FeVO_4$. In addition, the acidic FeO_x sites become almost completely covered by surface VO_x sites. This is demonstrated by depositing a monolayer of redox surface VO_x species on the acidic α-Fe_2O_3 support to yield a totally redox catalytic material with almost the same surface chemical characteristics (N_s, k_{rds}, and TOF_{redox}). Consequently, the interactions between anisotropic V_2O_5 and isotropic α-Fe_2O_3 forms isotropic $FeVO_4$ and significantly increases the number density of catalytic sites relative to the anisotropic V_2O_5 morphology, as well as creates catalytic materials predominantly containing redox surface VO_x sites.

dx.doi.org/10.1021/cs1000569 |ACS Catal. 2011, 1, 54–66

4.5. Surface Chemistry and Lattice Oxygen Diffusion of Bulk $FeVO_4$. As already mentioned above, the surface chemistry of iron-vanadate catalysts is determined by the nature of the exposed catalytic active sites, which are redox surface VO_x species. The surface FeO_x sites do not possess significant redox character because they are only mildly reducible and, as a result, are only able to convert a minor amount of the surface CH_3O^* and CH_3OH^* intermediates to HCHO during CH_3OH-TPSR. In contrast, bulk $FeVO_4$, as well as all the V-containing catalysts, possess redox surface VO_x sites that readily convert both the surface CH_3O^* and CH_3OH^* intermediates to HCHO.

The cyclic CH_3OH-TPSR experiments with bulk $FeVO_4$ in the absence of gas-phase molecular O_2 reveal that the redox surface VO_x sites are employing lattice oxygen for the oxidation of the surface reaction intermediates to HCHO, which is known as the Mars−van Krevelen mechanism.[36] The constant T_p value during the CH_3OH-TPSR cycles obtained from the bulk $FeVO_4$ clearly reveals that the surface VO_x sites remain fully oxidized by the supply of bulk lattice oxygen since the T_p value is known to significantly increase as the surface cation sites become reduced.[35] The fully oxidized surfaces indicate that the diffusion of oxygen from the $FeVO_4$ bulk lattice is relatively rapid since the catalysts were only briefly exposed to mild temperatures ($T < 400$ °C). The area under the CH_3OH-TPSR curves also remains constant reflecting complete reoxidation of the surface sites by *bulk* lattice oxygen.

4.6. Kinetics. The CH_3OH-TPSR T_p temperatures for the V-containing catalysts are very similar with T_p varying from ~195−201 °C reflecting the dominance of the redox surface VO_x sites in bulk V_2O_5 and $FeVO_4$ and the supported 4% V_2O_5/α-Fe_2O_3 catalyst. The CH_3OH-TPSR T_p value reflects the kinetics for breaking the C−H bond of the surface CH_3O^* intermediate and probably also the intact surface CH_3OH^* species. The methanol adsorption characteristics are reflected in the K_{ads} values given in Table 2 and are also comparable, within a factor of 2, for the V-containing catalysts. All the V-containing catalysts operate via a Mars−van Krevelen mechanism that is zero-order in O_2 partial pressure by employing lattice oxygen[36] as was previously also found for other supported V_2O_5 catalysts for a host of oxidation reactions.[42−47] The comparable CH_3OH adsorption equilibrium (K_{ads}) values and rate-determining-step kinetic (k_{rds}) values for V−OCH_3^* decomposition to HCHO over bulk V_2O_5, supported V_2O_5/α-Fe_2O_3 and $FeVO_4$ reveals that the overall kinetics for methanol oxidation are comparable over surface VO_x sites in these three catalytic systems. Consequently, the surface VO_4 sites on the bulk $FeVO_4$ mixed metal oxide represent the catalytic active sites for methanol oxidation to formaldehyde.

5. CONCLUSIONS

A phase-pure, bulk $FeVO_4$ catalyst was synthesized by co-precipitation and confirmed with Raman spectroscopy and TEM analysis that secondary crystalline V_2O_5 and α-Fe_2O_3 phases are not present. Both intact surface CH_3OH^* and CH_3O^* are present on bulk α-Fe_2O_3 exposed to methanol at 100 °C and yield CH_3OH and DME as reaction products, respectively. The surface intermediates primarily yield HCHO for the bulk V_2O_5 and $FeVO_4$ catalysts. Thus, formation of HCHO during methanol oxidation requires the presence of surface vanadium oxide sites, which are the dominant active redox component for the bulk $FeVO_4$ catalyst. The HR-TEM images and EELS analysis reveal that an amorphous VO_x-rich layer of ~1 nm exists on the outer surface of bulk $FeVO_4$.

The role of surface VO_x sites for methanol oxidation to formaldehyde was also examined with a model supported 4% V_2O_5/α-Fe_2O_3 catalyst consisting of a surface VO_x monolayer of mono-oxo O=VO_3 coordination. The surface CH_3O^* and CH_3OH^* intermediates on the supported VO_4 monolayer on α-Fe_2O_3 yielded HCHO as the major reaction product, which reflects its redox surface nature. Comparison of the findings for the surface VO_4 monolayer on α-Fe_2O_3 support and bulk $FeVO_4$ further indicates that surface VO_4 sites are the catalytic active sites for methanol oxidation over the bulk $FeVO_4$ catalyst. Moreover, the steady-state catalytic performance of the supported 4% V_2O_5/α-Fe_2O_3 catalyst is found to be comparable to that of the bulk $FeVO_4$ catalyst. The methanol oxidation reaction over the V-containing catalysts proceeds via a Mars-van Krevelen mechanism employing bulk lattice oxygen, which is replenished by gas phase molecular O_2.

■ ASSOCIATED CONTENT

Ⓢ Supporting Information. Figure showing the SAED pattern of the model-supported V_2O_5/α-Fe_2O_3 catalyst. This information is available free of charge via the Internet at http://pubs.acs.org/.

■ AUTHOR INFORMATION

Corresponding Author
*E-mail: iew0@lehigh.edu.

■ ACKNOWLEDGMENT

The financial support provided by the U.S. Department of Energy-Basic Energy Sciences (Grant DE-FG02-93ER14350) for this research is gratefully acknowledged. We would also like to acknowledge C.J. Keturakis (Operando Molecular Spectroscopy & Catalysis Laboratory, Lehigh University) for collecting the IR spectra of the supported 4% V_2O_5/α-Fe_2O_3 catalyst.

■ REFERENCES

(1) Grasselli, R. K.; Burrington, J. D. *Adv. Catal.* **1981,** *30,* 133–163.
(2) Adkins, H.; Peterson, W. R. *J. Am. Chem. Soc.* **1931,** *53,* 1512–1520.
(3) Botella, P.; Lopez Nieto, J. M.; Dejoz, A.; Vazquez, M. I.; Martinez-Arias, A. *Catal. Today* **2003,** *78,* 507–512.
(4) Pyrz, W. D.; Blom, D. A.; Shiju, N. R.; Guliants, V. V.; Vogt, T.; Buttrey, D. J. *Catal. Today* **2009,** *142,* 320–328.
(5) Wachs, I. E. *Catal. Today* **2005,** *100,* 79–94.
(6) Ballarini, N.; Cavani, F.; Cortelli, C.; Ligi, S.; Pierelli, F.; Trifiro, F.; Fumagalli, C.; Mazzoni, G.; Monti, T. *Top. Catal.* **2006,** *38,* 147–156.
(7) Briand, L. E.; Tkachenko, O. P.; Guraya, M.; Gao, X.; Wachs, I. E.; Grunert, W. *J. Phys. Chem. B* **2004,** *108,* 4823–4830.
(8) Merzlikin, S. V.; Tolkachev, N. N.; Briand, L. E.; Strunskus, T.; Wöll, C.; Wachs, I. E.; Grünert, W. *Angew. Chem., Int. Ed.* **2010,** *49,* 8037–8041.
(9) Guliants, V. V.; Bhandari, R.; Brongersma, H. H.; Knoester, A.; Gaffney, A. M.; Han, S. *J. Phys. Chem. B* **2005,** *109,* 10234–10242.
(10) Briand, L. E.; Jehng, J.-M.; Cornaglia, L.; Hirt, A. M.; Wachs, I. E. *Catal. Today* **2003,** *78,* 257–268.
(11) Wachs, I. E.; Briand, L. E. U.S. Patent 7 193 117 B2 (2007), March 20, 2007.
(12) Tian, H.; Wachs, I. E.; Briand, L. E. *J. Phys. Chem. B* **2005,** *109,* 23491–23499.

(13) Burcham, L. J.; Briand, L. E.; Wachs, I. E. *Langmuir* **2001,** *17*, 6175–6184.
(14) Routray, K.; Briand, L. E.; Wachs, I. E. *J. Catal.* **2008,** *256*, 145–153.
(15) Tatibouët, J. M. *Appl. Catal., A* **1997,** *148*, 213–252.
(16) Badlani, M.; Wachs, I. E. *Catal. Lett.* **2001,** *75*, 137–149.
(17) Briand, L. E.; Hirt, A. M.; Wachs, I. E. *J. Catal.* **2001,** *202*, 268–278.
(18) Gao, X.; Bare, S. R.; Weckhuysen, B. M.; Wachs, I. E. *J. Phys. Chem. B* **1998,** *102*, 10842–10852.
(19) Watanabe, M.; Ackland, D. W.; Kiely, C. J.; Williams, D. B.; Kanno, M.; Hynes, R.; Sawada, H. *JEOL News* **2006,** *41*, 2–7.
(20) Briand, L. E.; Farneth, W.; Wachs, I. E. *Catal. Today* **2000,** *62*, 219–229.
(21) Demmin, R. A.; Gorte, R. J. *J. Catal.* **1984,** *90*, 32–39.
(22) Niemantsverdriet, J. W. *Spectroscopy in Catalysis*; Wiley-VCHVerlag GmbH: Weinheim, Germany, 2000; p 141.
(23) Döbler, J.; Pritzsche, M.; Sauer, J. *J. Am. Chem. Soc.* **2005,** *127*, 10861–10868.
(24) Routray, K.; Deo, G. *AIChE J.* **2005,** *51*, 1733–1746.
(25) Jehng, J.-M.; Wachs, I. E.; Clark, F. T.; Springman, M. C. *J. Mol. Catal.* **1993,** *81*, 63–75.
(26) Griffith, W. P.; Lesniak, P. J. B. *J. Chem. Soc. A* **1969,** *7*, 1066–1071.
(27) Routray, K.; Zhou, W.; Kiely, C. J.; Gruenert, W.; Wachs, I. E. *J. Catal.* **2010,** *275*, 84–98.
(28) Luo, J. *Crit. Rev. Solid State Mater. Sci.* **2007,** *32*, 67–109.
(29) Qian, H.; Luo, J. *Acta Mater.* **2008,** *56*, 4702–4714.
(30) Guliants, V. V.; Benziger, J. B.; Sunderesan, S.; Yao, N.; Wachs, I. E. *Catal. Lett.* **1995,** *32*, 379–386.
(31) Hutchings, G. J.; Bartley, J. K.; Webster, J. M.; Lopez-Sanchez, J. A.; Gilbert, D. J.; Kiely, C. J.; Carley, A. F.; Howdle, S. M.; Sajip, S.; Calderelli, S.; Rhodes, C.; Volta, J. C.; Poliakoff, M. *J. Catal.* **2001,** *197*, 232–235.
(32) Bluhm, H.; Havecker, M.; Kleimenov, E.; Knop-Gericke, A.; Liskowski, A.; Schlogl, R.; Su, D. S. *Top. Catal.* **2003,** *23*, 99–107.
(33) Kiely, C. J.; Sajip, S.; Ellison, I. J.; Sananes, M. T.; Hutchings, G. J.; Volta, J. C. *Catal. Lett.* **1995,** *33*, 357–368.
(34) Burcham, L. J.; Briand, L. E.; Wachs, I. E. *Langmuir* **2001,** *17*, 6164–6174.
(35) Wachs, I. E.; Jehng, J.-M.; Ueda, W. *J. Phys. Chem. B* **2005,** *109*, 2275–2284.
(36) Mars, P.; van Krevelen, D. W. *Chem. Eng. Sci.(Spec. Suppl)* **1954,** *3*, 41–57.
(37) Liu, H. C.; Iglesia, E. *J. Catal.* **2004,** *223*, 161–169.
(38) Kurzawa, M.; Tomaszewicz, E. *Spectrochim. Acta, Part A* **1999,** *55*, 2889–2892.
(39) Knozinger, H.; Taglauer, E. *Catalysis* **1993,** *10*, 1–40.
(40) Wang, C.-B.; Cai, Y.; Wachs, I. E. *Langmuir* **1999,** *15*, 1223–1235.
(41) Arora, N.; Deo, G.; Wachs, I. E.; Hirt, A. M. *J. Catal.* **1996,** *159*, 1–13.
(42) Wachs, I. E.; Deo, G.; Weckhuysen, B. M.; Andreini, A.; Vuurman, M. A.; de Boer, M.; Amiridis, M. D. *J. Catal.* **1996,** *161*, 211–221.
(43) Wachs, I. E.; Jehng, J.-M.; Deo, G.; Weckhuysen, B. M.; Guliants, V. V.; Benziger, J. B.; Sundaresan, S. *J. Catal.* **1997,** *170*, 75–88.
(44) Chen, K.; Khodakov, A.; Yang, J.; Bell, A. T.; Iglesia, E. *J. Catal.* **1999,** *186*, 325–333.
(45) Zhao, C.; Wachs, I. E. *J. Phys. Chem. C* **2008,** *112*, 11363–11372.
(46) Routray, K.; Reddy, K. R. S. K.; Deo, G. *Appl. Catal., A* **2004,** *265*, 103–113.
(47) Dunn, J. P.; Koppula, P.; Stenger, H. G.; Wachs, I. E. *Appl. Catal., B* **1998,** *19*, 103–117.